JOURNAL OF GEOPHYSICAL RESEARCH, VOL. 91, NO. D12, PAGES 13,167–13,185, NOVEMBER 20, 1986

Transport of Atmospheric Tracers by Planetary Waves During A Winter Stratospheric Warming Event: A Three-Dimensional Model Simulation

W. KOUKER

Max Planck Institute for Chemistry, Mainz, Federal Republic of Germany

G. BRASSEUR[1]

National Center for Atmospheric Research, Boulder, Colorado

In a simple three-dimensional primitive equation model, a wave number 1 major stratospheric warming is simulated. With the aid of two idealized tracers it is shown that the transport during a major warming event is characterized by a small, well-organized tongue of subtropical air flowing around the displaced winter vortex into the polar cap and by a wide area with strong quasi-horizontal mixing (surf zone). The description of these dynamical processes requires a full three-dimensional space resolution.

1. INTRODUCTION

The chemistry and transport of atmospheric trace species have been extensively studied over the last decade. A number of numerical models have been developed to understand the key processes governing the behavior of these species and to assess the potential effects of human activities on the chemical composition of the stratosphere and especially on the ozone layer. Classical one-dimensional models, which assume perfect horizontal homogeneity and parameterize the vertical exchanges through a simple eddy diffusion process, are appropriate to investigate the relative importance of the chemical and photochemical reactions which partly determine the distribution of the trace species. Two-dimensional models consider the latitudinal and seasonal variations of insolation and the effect of meridional transport. These models are based on the zonally averaged energy, momentum, and continuity equations, in which the effect of zonal asymmetries (eddies) on the mean meridional transport has to be parameterized. In the so-called eulerian two-dimensional models [*Hesstvedt*, 1973; *Louis*, 1974; *Crutzen*, 1975; *Harwood and Pyle*, 1975; *Whitten et al.*, 1977; *Brasseur and Bertin*, 1977, 1979] the eddy fluxes are related to the zonally averaged quantities in terms of eddy diffusion coefficients obtained under the linear assumptions of the mixing length model of *Reed and German* [1965]. At certain occasions and certain locations the transport by the eddies dominates the transport by the eulerian mean circulation. This explains, for example, why ozone, which is produced at low latitudes, is transported towards the pole despite the equatorward flow in the stratosphere associated with the Ferrell cell, which is present at mid- and high latitudes. A close examination of the momentum and heat budgets reveals a large degree of cancellation between the eulerian mean and eddy transports. This cancellation, which is a consequence of the nonacceleration theorem [*Charney and Drazin*, 1961; *Andrews and McIntyre*, 1976, 1978; *Holton*, 1980] is an artifact of the eulerian zonal averages in pressure or geometric coordinates. Such representation leads to practical problems, as it has to be expressed by the difference between two large and approximately equal contributions. Therefore alternative formulations have been used. *Tung* [1982] and *Ko et al.* [1985] have shown, for example, that eulerian average equations, formulated in isentropic coordinates, can be constructed without giving rise to this problem of large mean/eddy transport cancellation. *Andrews and McIntyre* [1976], *Dunkerton* [1978], and *Holton* [1981] have indicated that a more satisfactory separation between mean and eddy effects can be achieved through the transformed eulerian (or residual) circulation ($\bar{v}^*$, $\bar{w}^*$) which is defined by

$$\bar{v}^* = \bar{v} - \frac{1}{\rho_0}\frac{\partial}{\partial z}\left(\frac{\rho_0 \overline{v'\theta'}}{\partial\theta/\partial z}\right)$$

$$\bar{w}^* = \bar{w} + \frac{1}{a\cos\phi}\frac{\partial}{\partial\phi}\left(\cos\phi\,\frac{\overline{v'\theta'}}{\partial\bar{\theta}/\partial z}\right)$$

where $\bar{v}$ and $\bar{w}$ are the meridional and vertical components of the eulerian circulation, ϕ and z are the latitude and the altitude, respectively, θ is the potential temperature, and a is the earth's radius. The primes refer to the departure from the zonally averaged values, which are expressed by overbars. According to the noninteraction theorem, the transformed eulerian circulation has the important property of vanishing for steady and conservative waves. In the absence of radiative equilibrium conditions, as a result, for example, of wave activity, there will no longer be an exact, but a near-cancellation, between the eulerian mean and the mean and the eddy transport. A residual circulation ($\bar{v}^*$, $\bar{w}^*$) arises and, to a good approximation, is equivalent to the diabatic circulation, whose vertical velocity is directly proportional to the net heating rate. Such models, with a diabatically driven or a residual circulation, have been used extensively in the last 5 years to describe the meridional transport of several trace species [*Pyle and Rogers*, 1980; *Miller et al.*, 1981; *Garcia and Solomon*, 1983; *Guthrie et al.*, 1984; *Stordal et al.*, 1985]. The assumption implicit in all these models is that the net dispersive effect of planetary waves is small and can be crudely described in terms of eddy diffusion. Transience and dissipation can

[1]On leave from the Belgian Institute for Space Aeronomy, Brussels, Belgium.

Paper number 6D0441.
0148-0227/86/006D-0441$05.00

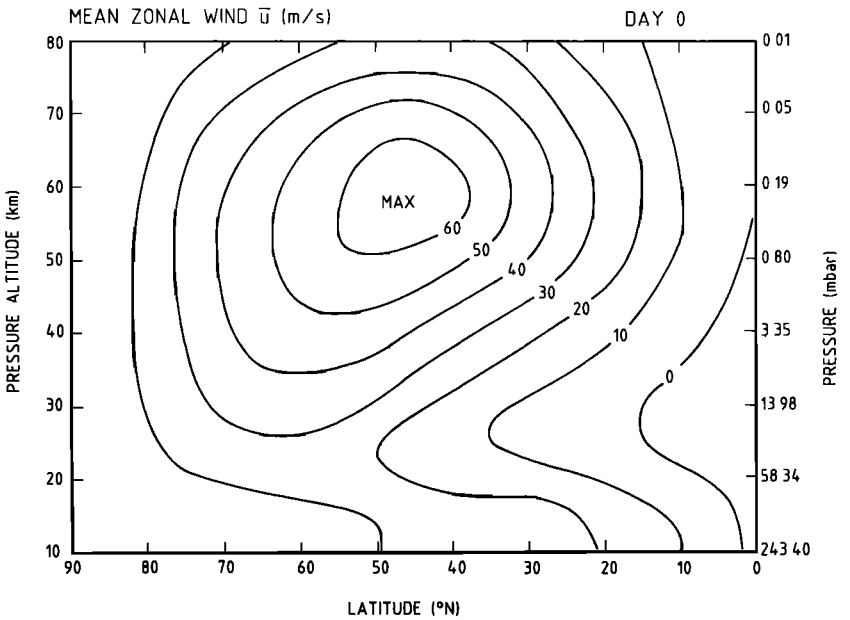

Fig. 1. Mean zonal wind (in meters per second) used as initial field, in geostrophic cyclostrophic and thermal wind balance.

become important in winter, especially during warming events. In this case some additional transport, not incorporated in the residual circulation, takes place. This is particularly true when irreversible mixing associated with planetary wave breaking occurs [*McIntyre and Palmer*, 1983]. Such nonlinear processes, whose quantitative importance on the large-scale dynamical structure of the atmosphere has been studied by *Rose* [1983], are believed to be responsible for a significant part of the eddy transport (together with chemical eddies) and are probably important in relation to the development of stratospheric warming events. Chemical eddy transport plays a large role in certain regions of the atmosphere for species (e.g., ozone) which have a sharp transition region between photochemically and dynamically dominated regimes.

The description of the meridional transport, as given by two-dimensional models, is thus in certain cases only a poor approximation. This is particularly true in the winter stratosphere, when the waves become unsteady and nonconservative. In this case the transport has to be studied by means of full three-dimensional models in which the behavior of planetary waves is treated explicitly.

It is now well established from observational studies that the transport of species with long chemical lifetimes, such as ozone in the lower stratosphere, is related to the variations of large-scale eddies [*Ghazi*, 1974; *Ghazi et al.*, 1976; *Gille*, 1979; *Leovy et al.*, 1985] and is even significantly enhanced at the time of stratospheric warmings [*Ghazi*, 1974]. Although the behavior of some minor constituents, such as ozone, has been considered in three-dimensional general circulation models [*Hunt and Manabe*, 1968; *Cunnold et al.*, 1975, 1980; *Mahlman and Moxim*, 1978; *Schlesinger and Mintz*, 1979; *Levy et al.*, 1979; *Mahlman et al.*, 1980] or in transport studies using marked parcels [*Kida*, 1977, 1983; *Hsu*, 1980; *Dunkerton et al.*, 1981], detailed representations of the tracer's transport during large perturbations such as warming events are few. *Hartmann and Garcia* [1979], *Garcia and Hartmann* [1980], and *Kawahira* [1982] have developed mechanistic quasi one-dimensional models of the ozone transport in the winter stratosphere, considering simple linear chemical and radiative feedback mechanisms.

In the present study the effect of forced waves on the transport of idealized tracers is considered in a full three-dimensional hemispheric nonlinear model. No chemical source is included, so that the only dissipative process (beside numerical filters) arises from the radiative net heating rate, which is parameterized by a simple linear relaxation term. The model is used to calculate the eulerian mean and the transformed eulerian mean meridional circulation. It is also shown that the transport of conservative tracers cannot be described in terms of purely zonally averaged flow, especially in winter when the planetary waves contribute significantly to the transport. In another study by *Rose and Brasseur* [1985] and *Brasseur and Rose* [1985] a chemical scheme involving oxygen, hydrogen, and nitrogen species was included in a similar simulation performed by a three-dimensional grid-point mechanistic model. The present model, however, is a semispectral mechanistic model and allows for a better zonal resolution, as it represents all waves up to wave number 7.

2. Model Description

The model which is used in the present study is a semispectral version of the grid-point three-dimensional hemispheric model developed at the Free University of Berlin by Rose and Klinker for the study of sudden stratospheric warmings [*Rose*, 1983]. It is based on the so-called primitive equations expressed in spherical coordinates [e.g., *Holton*, 1975] with $z = -H \ln (p/p_0)$ as the vertical coordinate (p is the pressure expressed in mbar, $p_0 = 1015.75$ mbar, and $H = 7$ km). This set of equations is truncated at zonal wave number 7 and is solved in a two-dimensional space of grid points with a meridional interval $\Delta\varphi = 5°$ and the vertical resolution of $\Delta z = 3$ km.

The southern boundary is located at the equator, where a mirror condition is applied. The upper boundary condition is specified by setting the vertical velocity equal to zero. As the

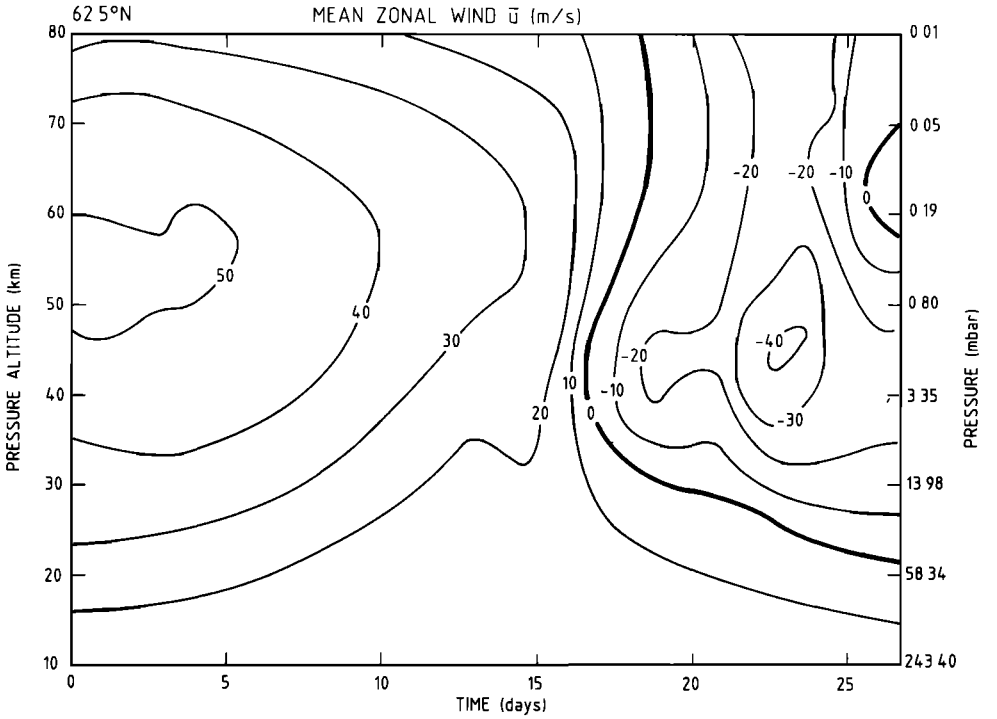

Fig. 2. Time-height cross section of the mean zonal wind (in meters per second) at 62.5°N during the course of the model integration.

forcing takes place at the lower boundary, the geopotential Φ at 8.5 km varies according to the following condition:

$$\Phi(n, \varphi, t) = f(t)h(\varphi)A^*(1)$$

where $h(\varphi) = 0$ for $\varphi \leq 30°$ and $\varphi \geq 82.5°$.

$$h(\phi) = \sin^2\{(\varphi - 30°)/[60° - (\varphi - 60°)/3]\} \qquad 30° < \varphi < 82.5°$$

$$f(t) = 1 - \exp(-\tau/\tau_0)$$

where $\tau_0 = 2.5 \times 10^5$ s. $A^*(1)$ is the maximum amplitude of the wave number 1 perturbation. For the prognostic variables the lower boundary condition corresponds to a no-wind shear condition and to a constant temperature of 215 K. The time integration is performed by a leapfrog scheme, with a time step of 7.5 min. To avoid separate evolutions at even and odd time steps, three time steps are performed at every forty-eighth time step, using the Euler-backward instead of the leapfrog scheme. Because of spherical geometry the zonal wavelength of a given wave number decreases with increasing latitude. Therefore in the northernmost latitude (87.5°N), only the zonal waves 1 and 2 are calculated in order to avoid linear instability without reducing the time step. To prevent the model from developing nonlinear instability, a method described by *Shapiro* [1971] is used by employing an eight-order

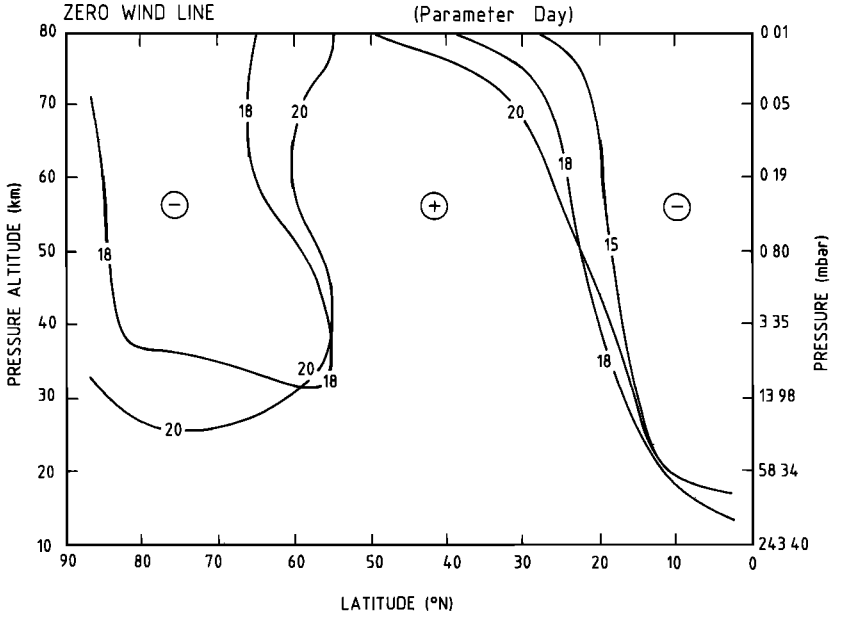

Fig. 3. Location in the meridional plane of the line where the mean zonal wind is equal to zero at day 15, 18, and 20 of the model integration.

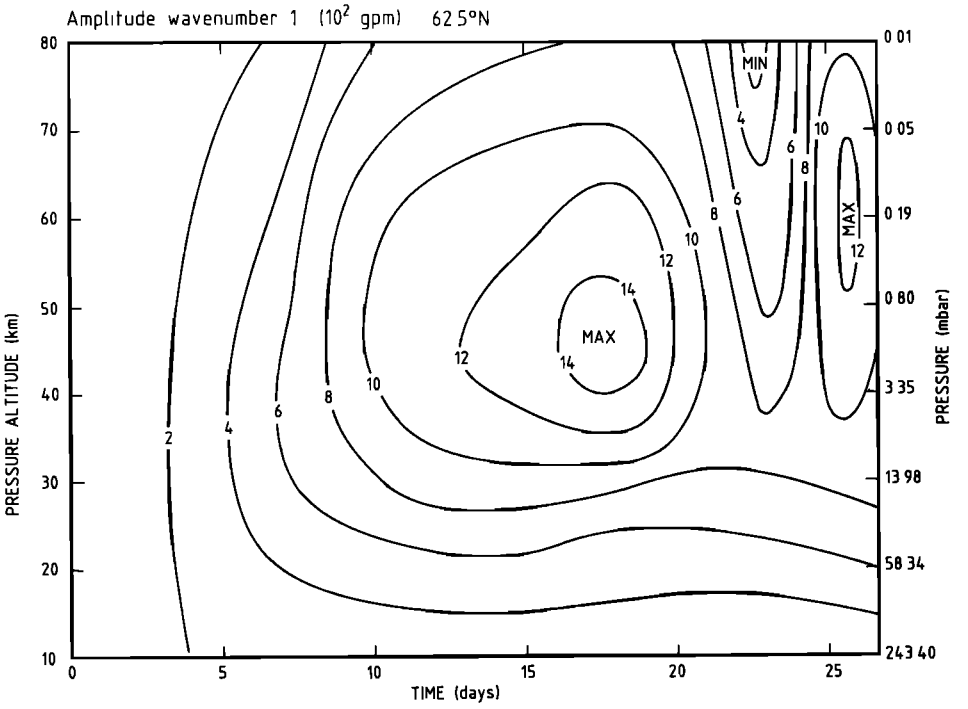

Fig. 4*a*.

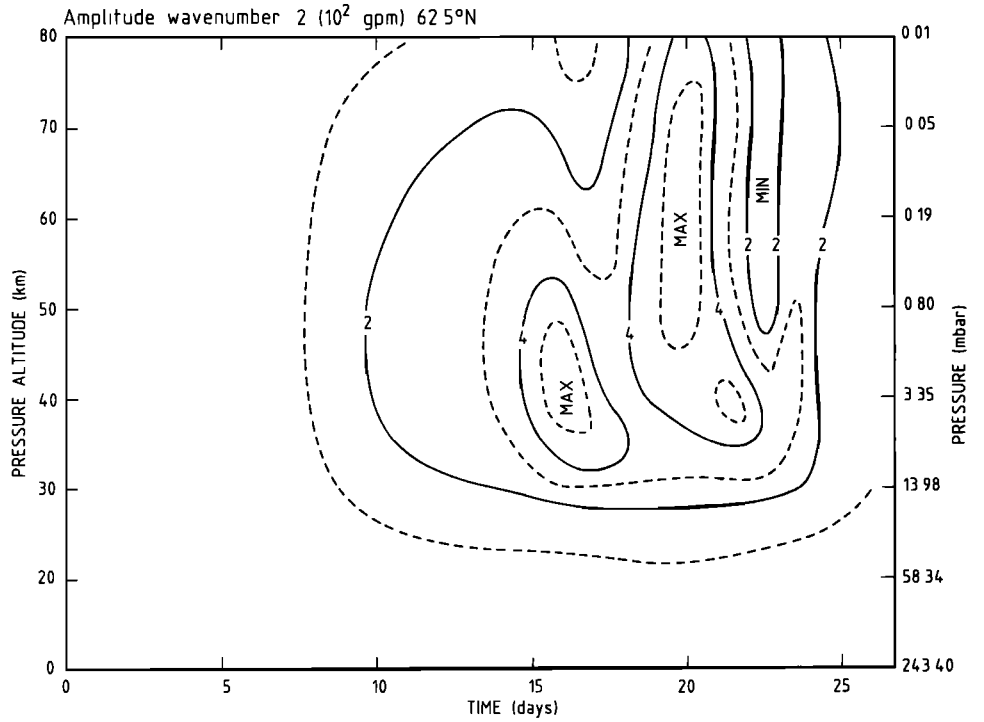

Fig. 4*b*.

Fig. 4. Time-height cross section of the (*a*) wave number 1 and (*b*) wave number 2 amplitude of the geopotential height (gpm) at 62.5°N during the course of the model integration.

filter in the north-south direction. In order to avoid reflection at the upper boundary, the order of the filter is reduced progressively up to the second order in the uppermost six levels.

3. Dynamical Parameters During a Stratospheric Warming Event

The model, as described in the section 2, is first used to calculate the dynamical parameters (wind components and temperature) in the winter hemisphere during the development of a warming event. At the initial stage the temperature and zonal wind distributions are assumed to be zonally symmetric (no wave) and are in mutual geostrophic cyclostrophic equilibrium (Figure 1). A wave number 1 forcing in the geopotential height (gpm) is applied at the lower boundary of the model, with a maximum amplitude of 300 gpm. This condition is intended to simulate the perturbations resulting from oro-

graphic or thermal processes in the troposphere. Stationary planetary waves are allowed to propagate in the stratosphere only in winter, when the zonal winds are westerly. In this case, only large-scale waves (wave number 1–3) are present, as can be deduced from the condition expressed by *Charney and Drazin* [1961]. These waves are expected to interact with the zonal wind through momentum deposition. Figure 2 shows the calculated evolution of the mean zonal winds as a function of height at 62.5°N, as a result of this wave-mean flow interaction. Its value, which is of the order of 50 m s^{-1} in the upper stratosphere and lower mesosphere decreases slowly during the first part of the integration, when the wave activity remains small; it reaches 40 m s^{-1} on day 8 and 30 m s^{-1} on day 14. During the next 5 days, as the waves become intense, the deceleration is enhanced, so that the mean zonal wind reverses on day 17 and reaches a value as large as -40 m s^{-1} at 45 km altitude on day 23. Such a situation is observed every one or two winters in the northern hemisphere (aside from the final warming) and is referred to as a major warming event. Figure 3 shows the position of the zero wind line ($\bar{u} = 0$) in the meridional plane for selected days. It appears that easterlies are present after day 15 in the tropical and high-latitude zones. In the latter region the calculated mean zonal wind, however, is significantly stronger than in the tropics.

The amplitude of the wave number 1 and 2 geopotential height variation at 62.5°N during the course of the integration is shown in Figures 4*a* and 4*b*. It can be seen that the amplitude of the wave number 1 height grows gradually during the first 15 days; it reaches 300 gpm on day 5, 800–1000 gpm between 35 and 70 km on day 10, and 1400 gpm near the stratopause on day 18. Later on, the strength of the wave decreases, expecially in the mesosphere, but increases again after day 25 during the final stage of the model integration. The time period with the largest wave number 1 amplitude (days 15–20) corresponds to the largest deceleration of the mean zonal wind and thus to the development of the warming event. The amplitude of wave number 1 starts to decrease as a critical line (zero wind line) becomes apparent.

The variation in the wave number 2 height remains limited during the first days of integration. Indeed, in the present model the forcing at the lower boundary is only a wave number 1 perturbation, and a wave number 2 response can only be produced by nonlinear processes which become significant as the warming develops. The amplitude of the wave number 2 geopotential height reaches maxima of about 400 gpm on day 16 and 20, respectively, but always remains significantly smaller than the wave number 1 amplitudes.

In order to represent the details of the wave structure at mid and high latitudes, Figures 5*a*–5*f* show synoptic maps of the geopotential height and the temperature at 11.6 mbar (~30 km) on days 15, 18, and 20, that is, in a layer and during a time period with large wave amplitudes. From Figure 5*a*, one sees that on day 15 the polar vortex is displaced from the pole, and as the wind blows nearly parallel to the isohypses, that meridional and vertical wind components appear. As a consequence, a strong cross-polar flow is observed. At day 18 the wave amplitude has become larger, and a high-pressure cell is now clearly visible at 180° longitude (Aleutian high). A similar situation is observed for day 20 of the simulation but with a high-pressure cell that has been displaced northwards.

The temperature distribution at the 11.6-mbar level for the same 3 days reveals a strong wave structure at mid and high latitudes, with an amplitude of nearly 50 K. A strong warming develops and is located on day 15 at about 50°N and 135°E. During the next days this warm cell (250 K) is slightly displaced northward and eastward. At the same time a cold air mass (205 K) is present at 70°N and 15°E. It is interesting to note that at day 15, when the warming is in its early stage, the temperature structure is quite regular and exhibits a "comma" shape. Three days later, an entire zone located in the western hemisphere at mid-latitude is characterized by a weak temperature gradient.

To conclude this part of the discussion, one should point out that the model is able to produce a major warming event in response to a tropospheric forcing. The dynamical structure associated with this warming event is in good qualitative agreement with observed wave number 1 events [*Petzoldt and Scholl*, 1986]. The model correctly simulates the displacement of the vortex, the formation of the Aleutian high-pressure cell, the reversal of the mean zonal wind at high latitude, and a temperature disturbance with an amplitude of about 50 K. Such behavior with transient and dissipative processes is expected to produce some net meridional transport, as will be discussed in section 4.

4. Meridional Circulation and Transport

The calculation of the zonally averaged meridional circulation resulting from the wave disturbances allows one to estimate the transport of heat and long-lived species. Most of these trace gases with a long chemical lifetime (e.g., ozone, nitric acid, nitrous oxide, methane, the chlorofluorocarbons) are produced or injected in the tropical stratosphere and transported toward the pole. Since the stationary planetary waves propagate only when the mean zonal wind is westerly, the strength of the mass flow is largest in winter and explains, for example, why the ozone amount at high latitudes is a maximum in early spring.

Figures 6*a*, 6*b*, and 6*c* represent, for example, the mass stream function corresponding to the eulerian mean circulation on days 15, 18, and 20. One clearly sees in the three cases the existence of a double-cell structure with upward motions in the tropics and above the pole and downward motions at mid-latitudes. Such a circulation is in good qualitative agreement with the meridional motions, based on observed winter data (see for example, *Vincent* [1968]). The indirect Ferrell cell, which produces an equatorward flux at high latitude in the stratosphere, remains strong during the course of the integration. This type of circulation, however, is not representative of the net heat and mass transport, as the zonally averaged flux of any quantity x is given by

$$\overline{vx} = \bar{v}\bar{x} + \overline{v'x'}$$

where the overbars refer to zonal means and the primes to the departure from this average (i.e., the eddies). Indeed, the eulerian mean meridional circulation corresponds only to the first term of the right-hand side of the above expression. The second term, which depends on the waves, introduces a contribution which nearly counterbalances the effect of the eulerian mean circulation when the dissipation is weak.

The residual circulation whose strength and direction is entirely different from the eulerian mean circulation is shown in Figures 7*a*, 7*b*, and 7*c* for days 15, 18, and 20. In this case the air flow is characterized by only one large cell, corresponding to an upward motion in the tropics, a large subsidence at high latitude, and a poleward flow in the entire stratosphere. The closed stream line, which is visible on days 18 and 20, is

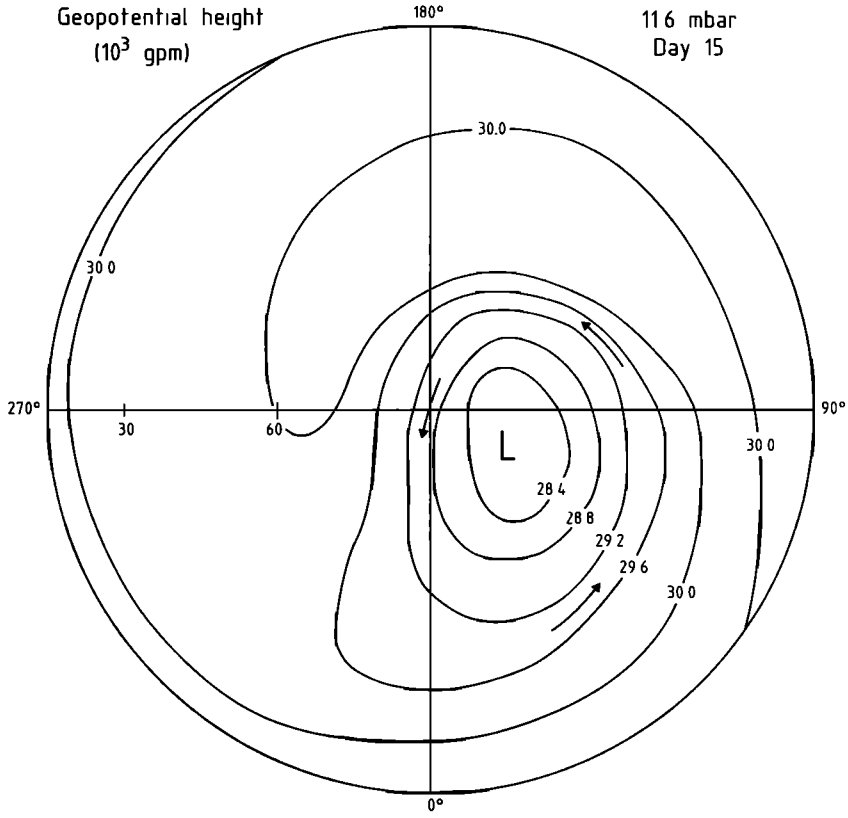

Fig. 5a.

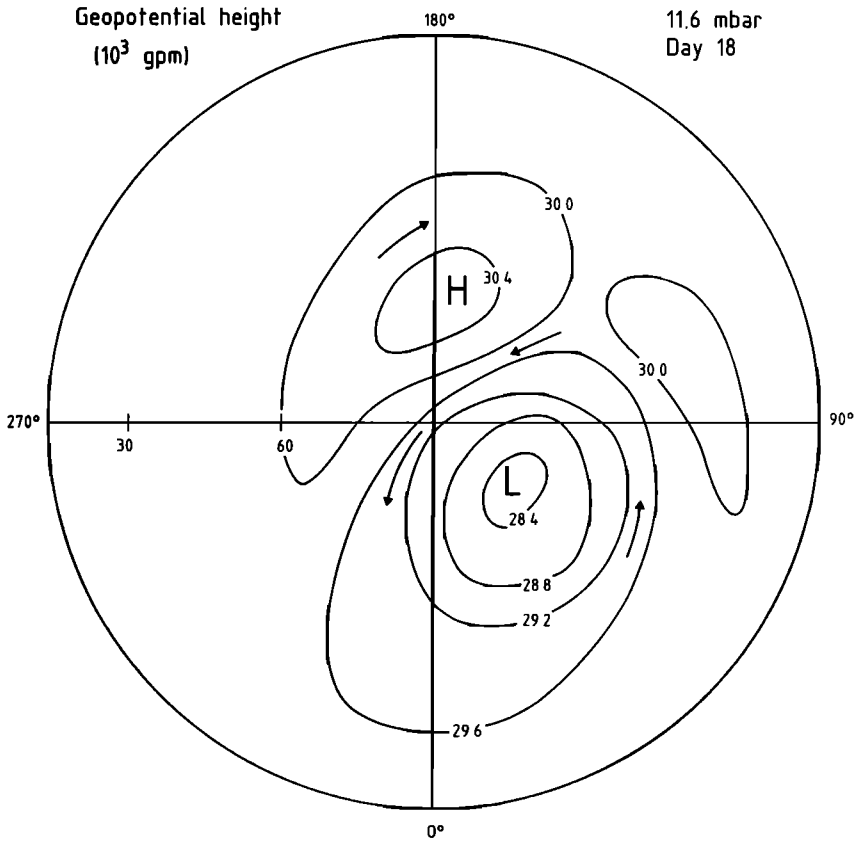

Fig. 5b.

Fig. 5. Synoptic charts of the geopotential height on (*a*) day 15, (*b*) day 18, and (*c*) day 20, and of the temperature on (*d*) day 15, (*e*) day 18, and (*f*) day 20, on the 11.6-mbar pressure surface.

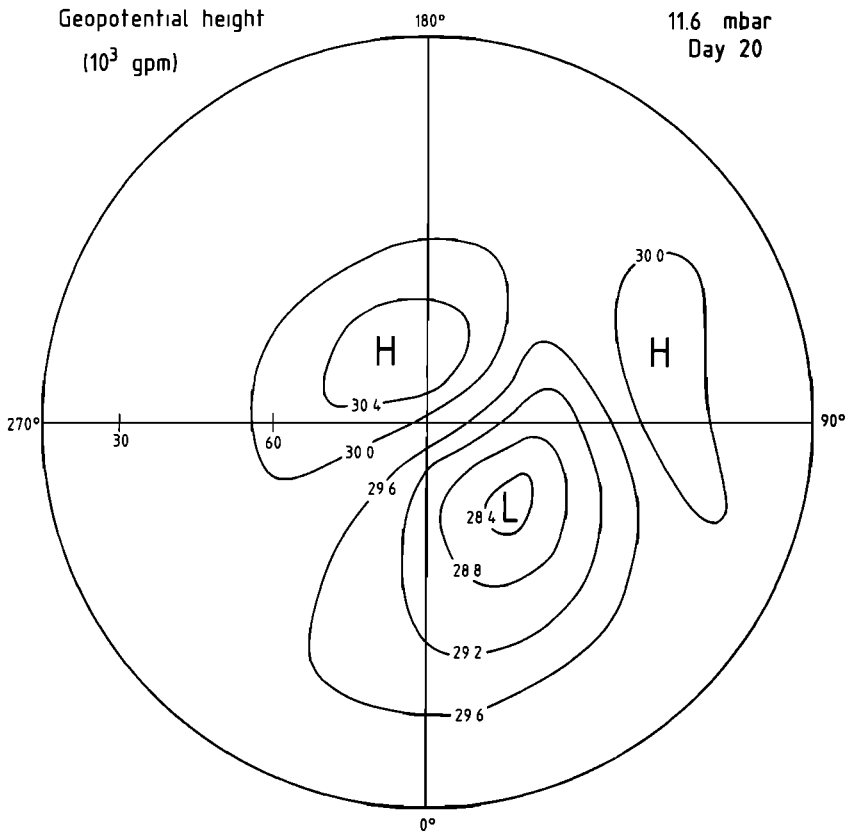
Geopotential height
(10³ gpm)
11.6 mbar
Day 20
180°
270°
90°
0°
30
60
H
H
L
30 0
30 4
30 0
29 6
28 4
28 8
29 2
29 6

Fig. 5c.

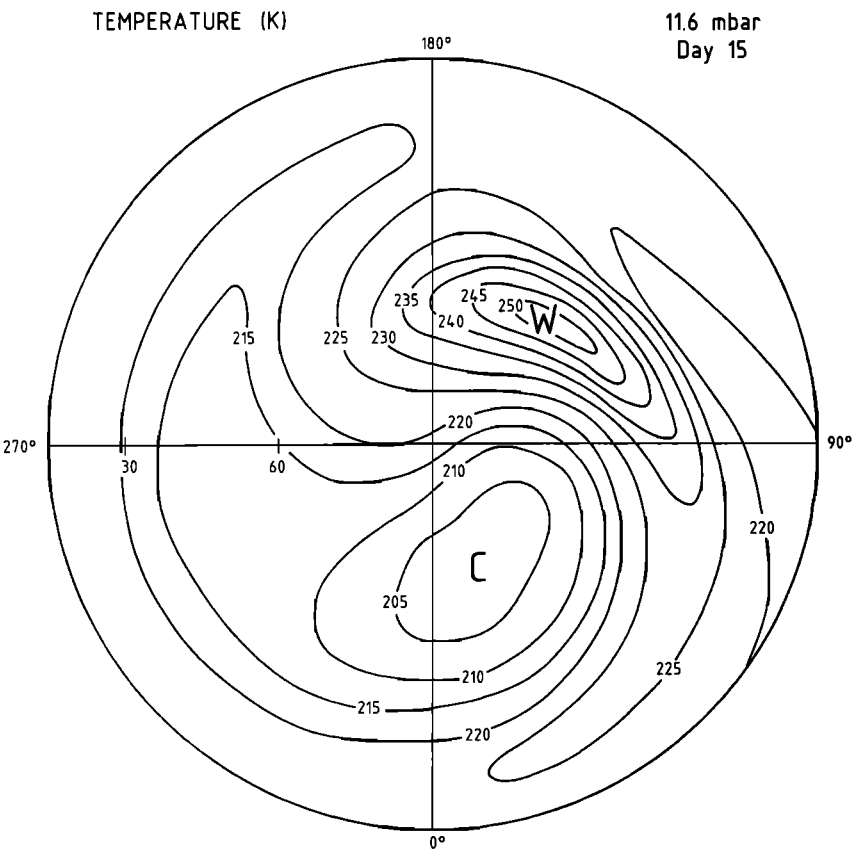
TEMPERATURE (K)
11.6 mbar
Day 15
180°
270°
90°
0°
30
60
W
C
215
225
230
235
240
245
250
220
210
205
215
210
220
225

Fig. 5d.

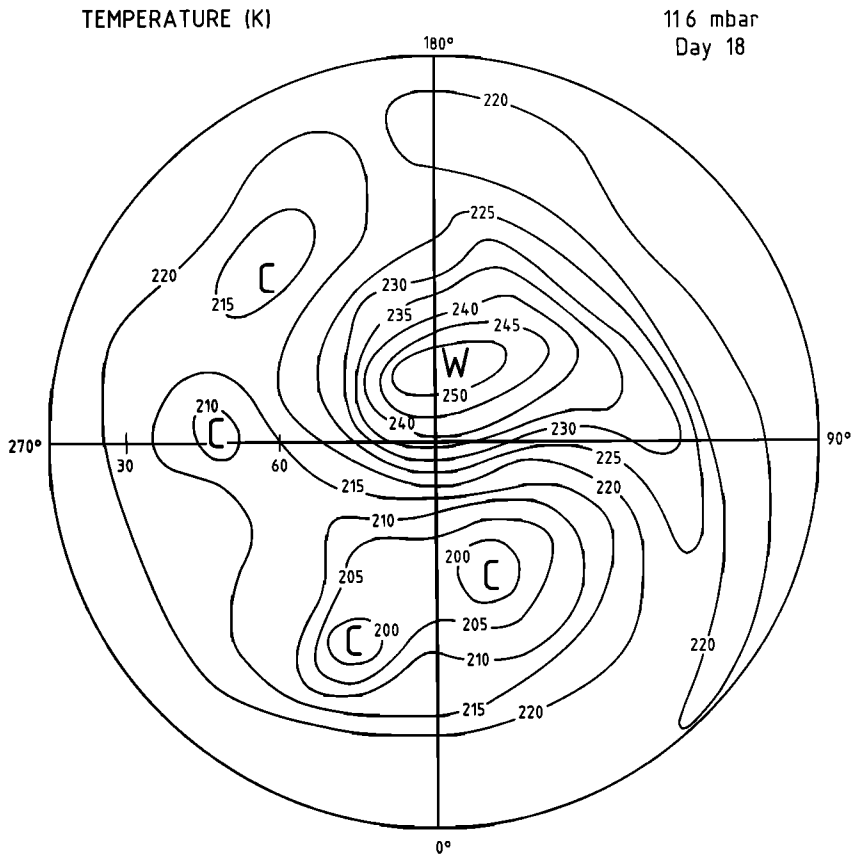
TEMPERATURE (K)
116 mbar
Day 18
180°
0°
270°
90°
30
60
220
225
230
235
240
245
250
215
210
205
200
W
C

Fig. 5e.

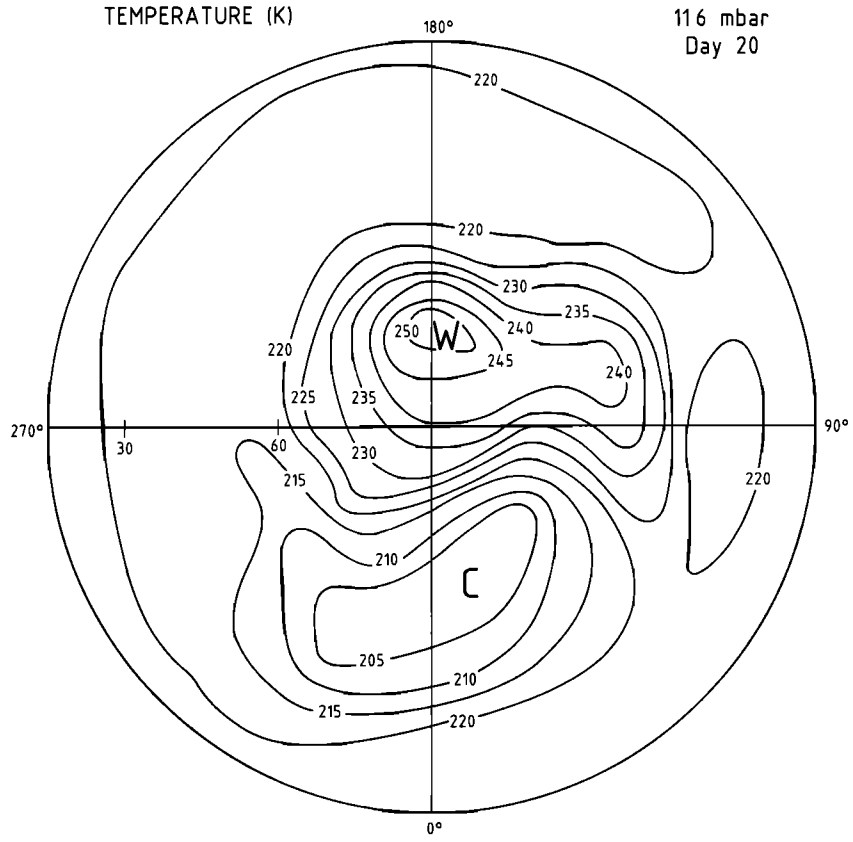
TEMPERATURE (K)
116 mbar
Day 20
180°
0°
270°
90°
30
60
220
225
230
235
240
245
250
215
210
205
W
C

Fig. 5f.

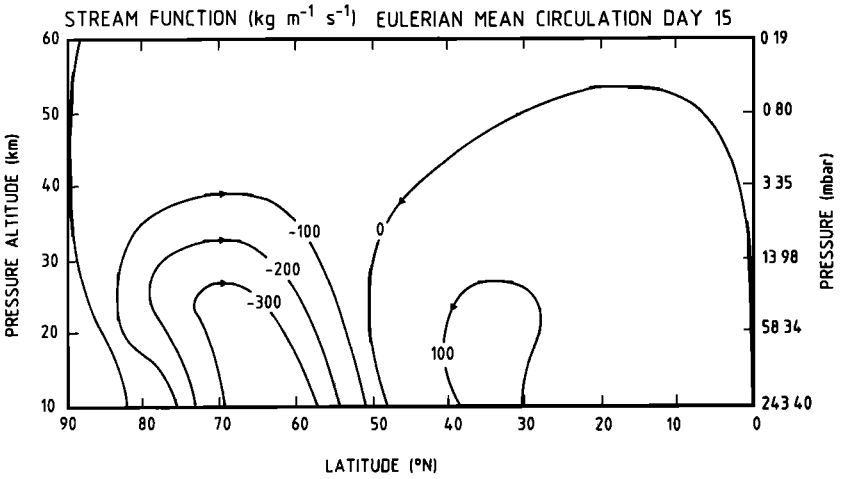

Fig. 6*a*

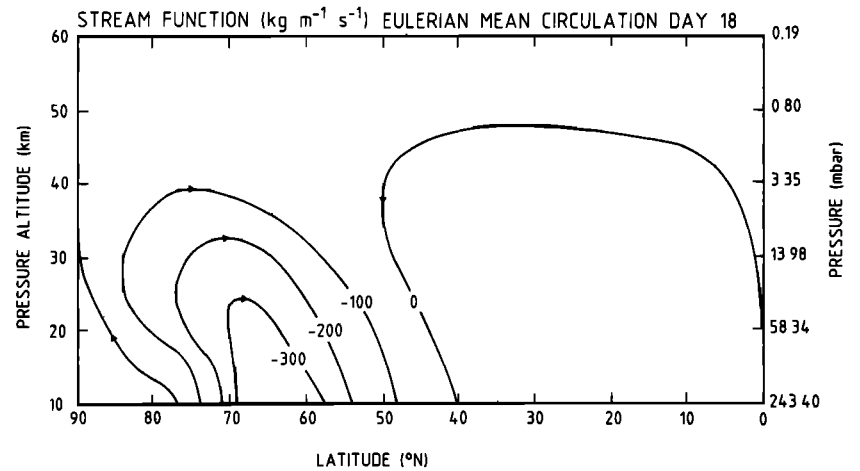

Fig. 6*b*

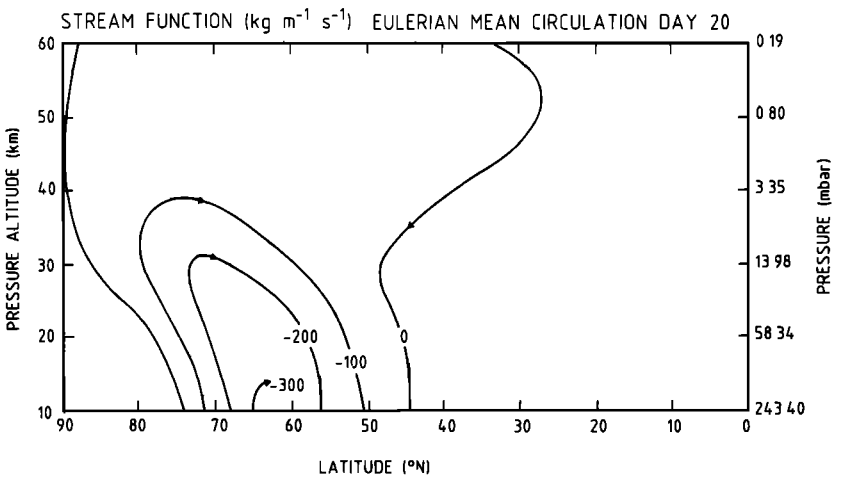

Fig. 6*c*

Fig. 6. Mass stream function (in kilograms per meter per second) of the eulerian zonal mean circulation on (*a*) day 15, (*b*) day 18, and (*c*) day 20 of the model simulation.

located just below the critical line of the zonal wind, which acts as a partial reflector of the planetary waves [*Dunkerton et al.*, 1981]. The residual circulation is similar to the earliest description of stratospheric motions based on observations of water vapor [*Brewer*, 1949] and ozone [*Dobson*, 1956]. It is also in qualitative agreement with the circulation deduced by *Murgatroyd and Singleton* [1961] and is based on the resolution of the thermodynamic equation in which the contribution of the eddy terms was omitted. In fact, the apparent discrepancy between the mean meridional circulations derived from

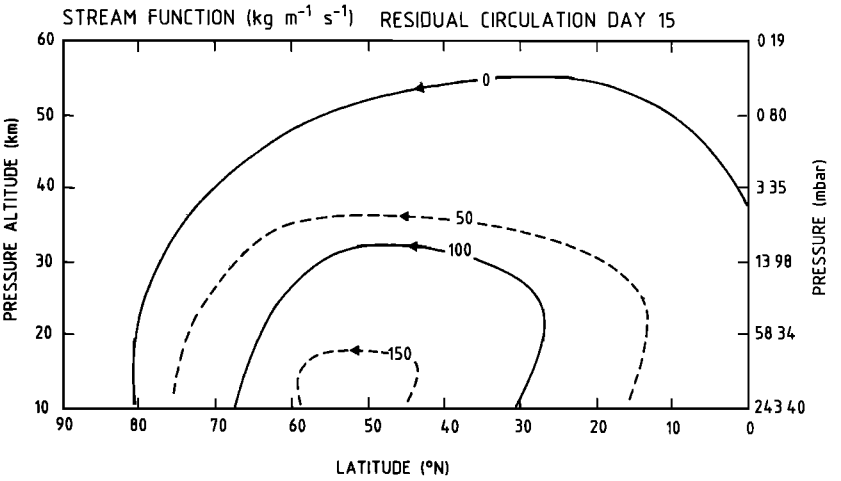

Fig. 7a.

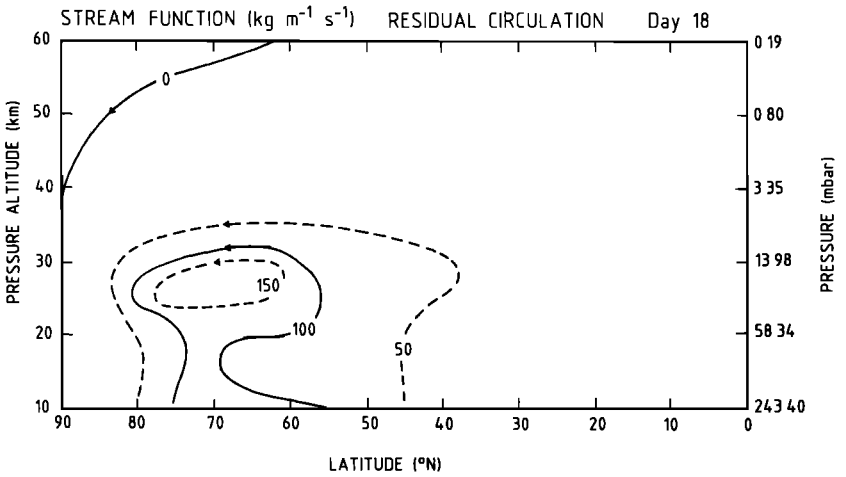

Fig. 7b.

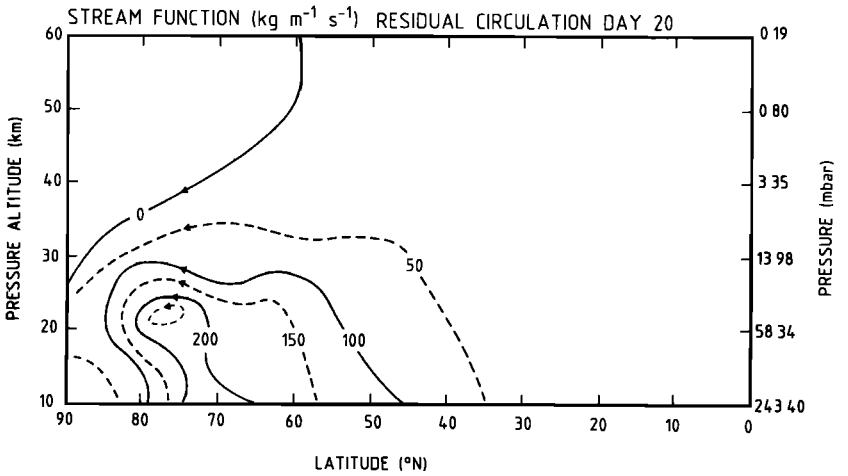

Fig. 7c.

Fig. 7. Mass stream function (in kilograms per meter per second) of the transformed eulerian mean circulation (residual circulation) on (*a*) day 15, (*b*) day 18, and (*c*) day 20 of the model simulation.

wind measurements and from trace species observations can be resolved by interpreting the first as eulerian mean motions and the second as an eulerian-transformed (or residual) circulation [see *Dunkerton*, 1978]. A more quantitative comparison is given in Figures 8*a* and 8*b*, which represent the vertical wind velocity on day 15 corresponding to the two types of averaging procedure. Again, large differences occur. In the case of the eulerian mean motions (Figure 8*a*) the vertical

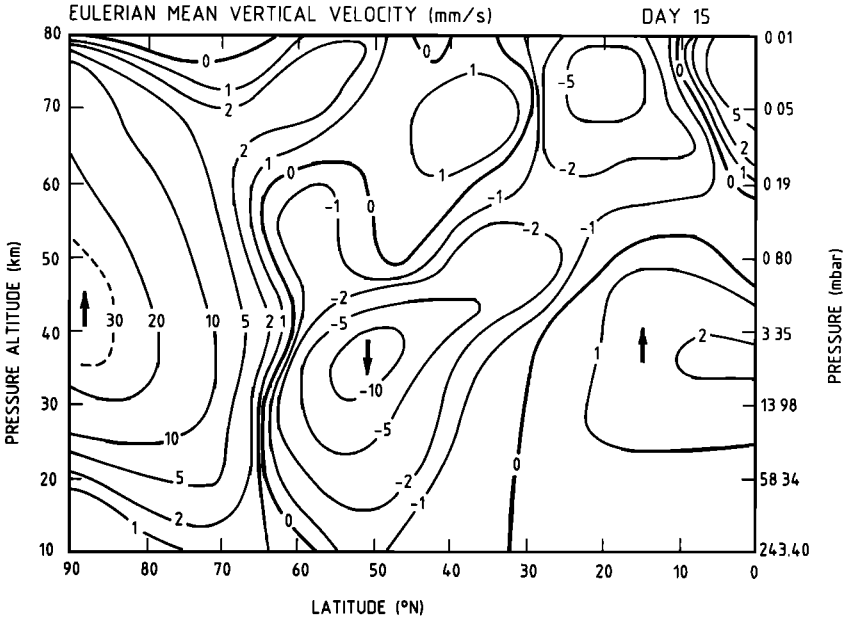

Fig. 8*a*.

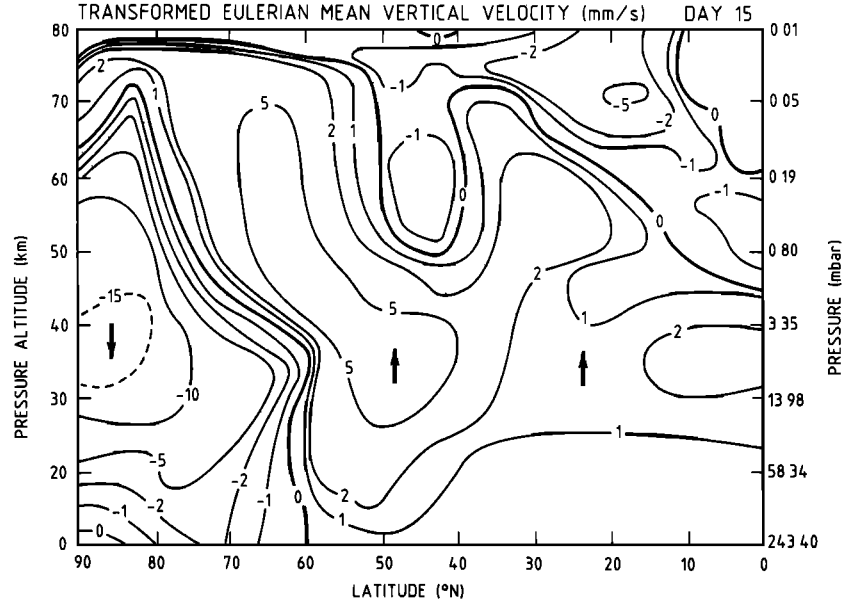

Fig. 8*b*.

Fig. 8. (*a*) Eulerian mean velocity and (*b*) transformed eulerian mean velocity of the vertial wind components (in millimeters per second) calculated on day 15 of the model simulation.

wind component is directed upward at latitude higher than 65°, with velocities of the order of 1 cm s^{-1}. In the case of the transformed mean circulation (Figure 8*b*), the wind is directed downward, with wind velocities also of the order of 1 cm s^{-1}. At low latitude the two motions are very similar, with upward winds of the order of 1–2 mm s^{-1}. Finally, at mid-latitude a clear downward wind is visible in the case of the eulerian mean circulation (1–10 mm s^{-1}), and a rather weaker upward motion (1–5 mm s^{-1}) occurs in the case of the transformed eulerian mean representation. It is important to note that during the simulation of a strong wave disturbance the transformed eulerian mean vertical component of the wind velocity is large at high latitude and that, despite the upward eulerian mean wind, the net transport of species is directed downward.

5. Transport of Conservative Tracers

In order to further study the transport in the winter stratosphere and, in particular, to determine the average meridional displacement of air parcels, the following numerical experiment has been performed. Two idealized, purely conservative tracers have been considered simultaneously. The mixing ratio of one of them, at the initial stage of integration, varies linearly with latitude from a value of 1 at the equator to an arbitrary 100 value at the pole. The initial distribution of this tracer is zonally symmetric and uniform with height. As the corresponding isolines for the mixing ratio are, in the meridional plane, parallel to the altitude axis, this tracer will be referred to as the meridionally stratified tracer.

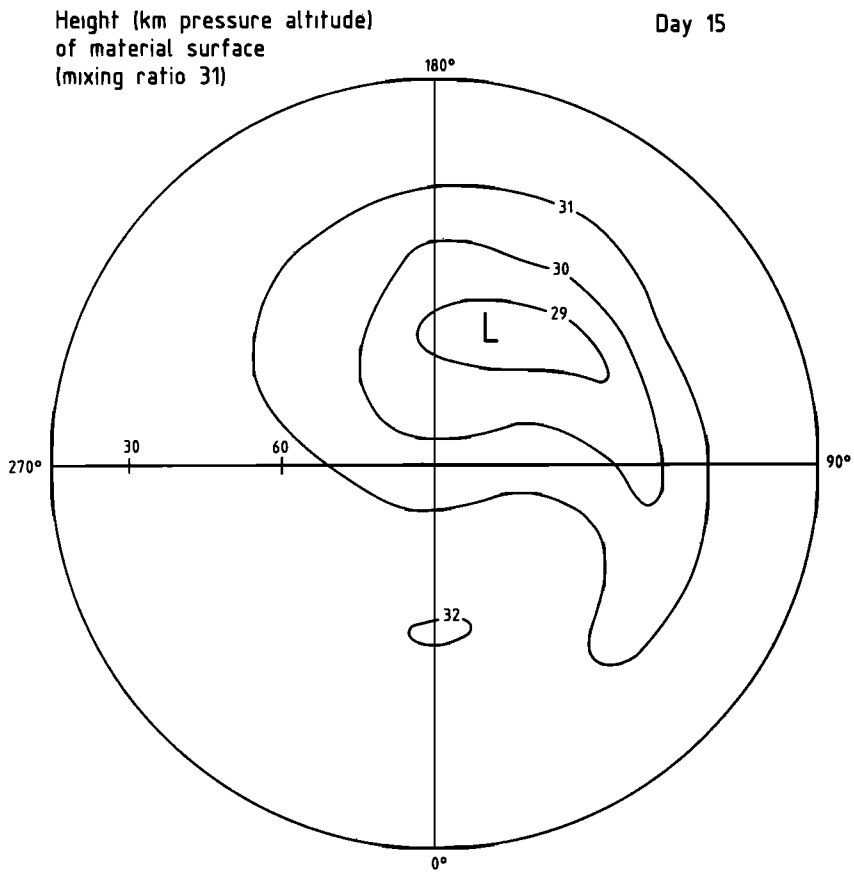

Fig. 9*a*.

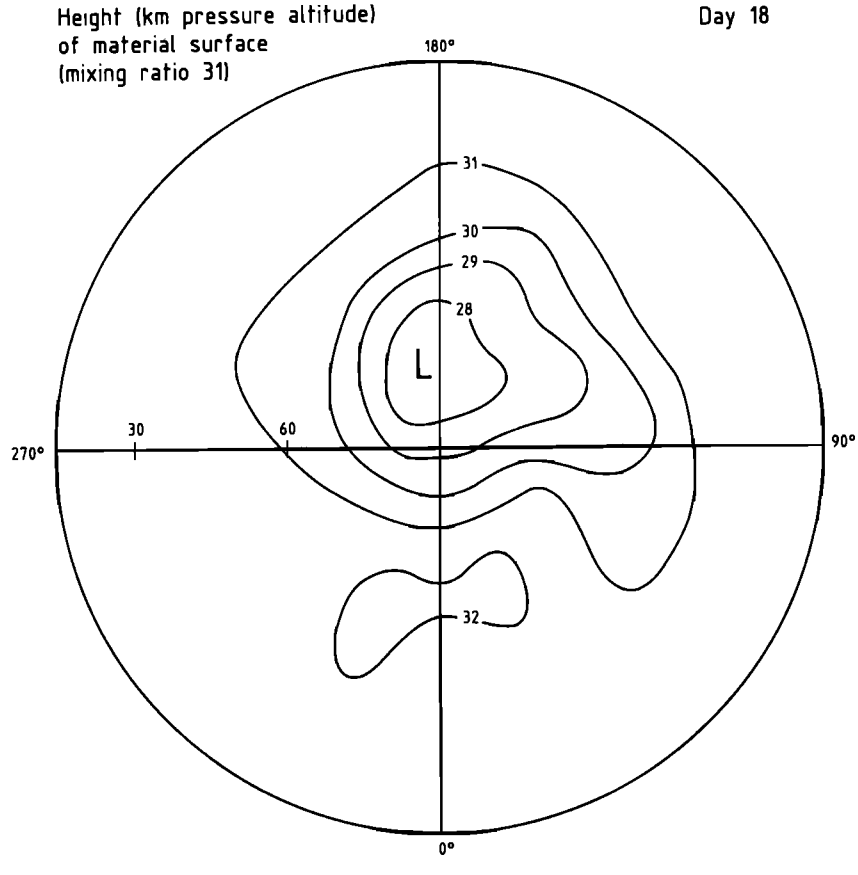

Fig. 9*b*.

Fig. 9. Synoptic representation of transport near 30 km altitude on (*a*) day 15, (*b*) day 18, and (*c*) day 20 of the model integration, and height (in kilometer pressure altitude) of a material surface which initially coincides with a pressure surface on (*d*) day 15, (*e*) day 18, and (*f*) day 20. Material lines initially parallel to latitude circles interpolated on the material surfaces are shown in Figures 9*a*–9*c*.

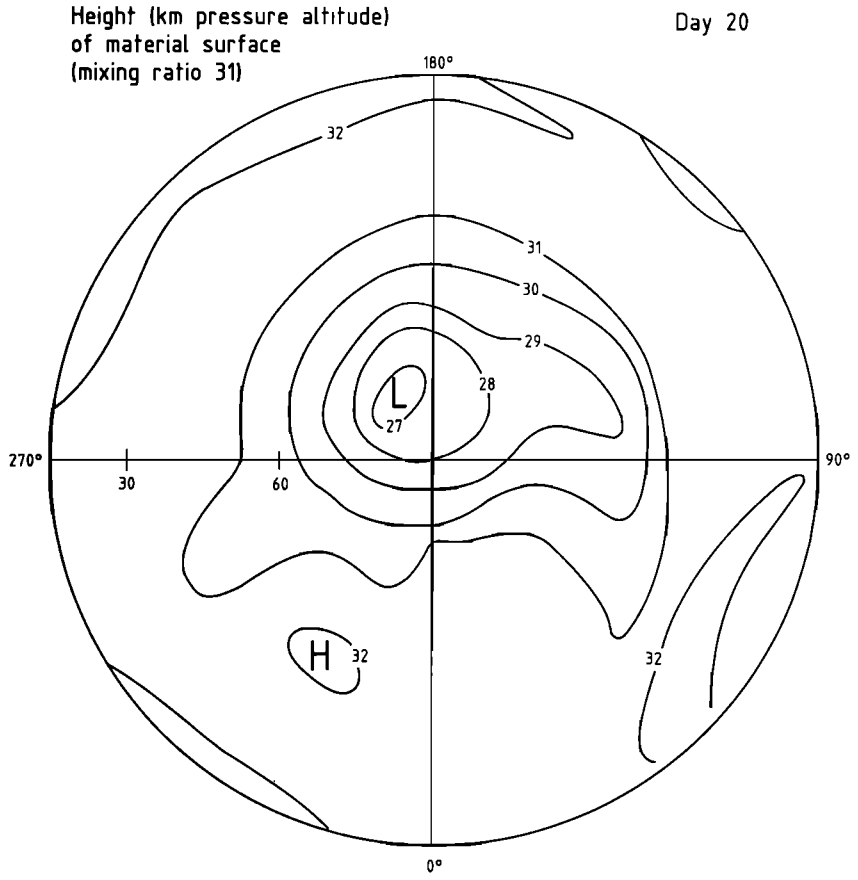
Height (km pressure altitude)
of material surface
(mixing ratio 31)
Day 20
180°
32
31
30
29
28
L
27
270°
30
60
90°
H
32
32
0°

Fig. 9*c*.

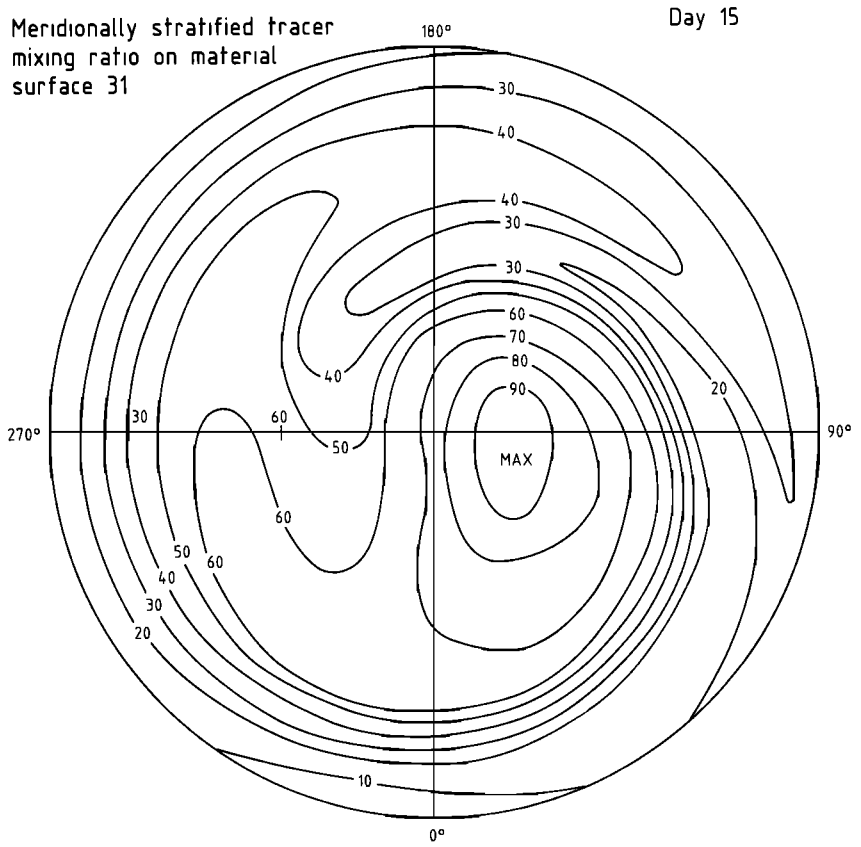
Meridionally stratified tracer
mixing ratio on material
surface 31
Day 15
180°
30
40
40
30
30
60
70
80
90
MAX
40
20
270°
30
60
50
90°
60
50
60
40
30
20
10
0°

Fig. 9*d*.

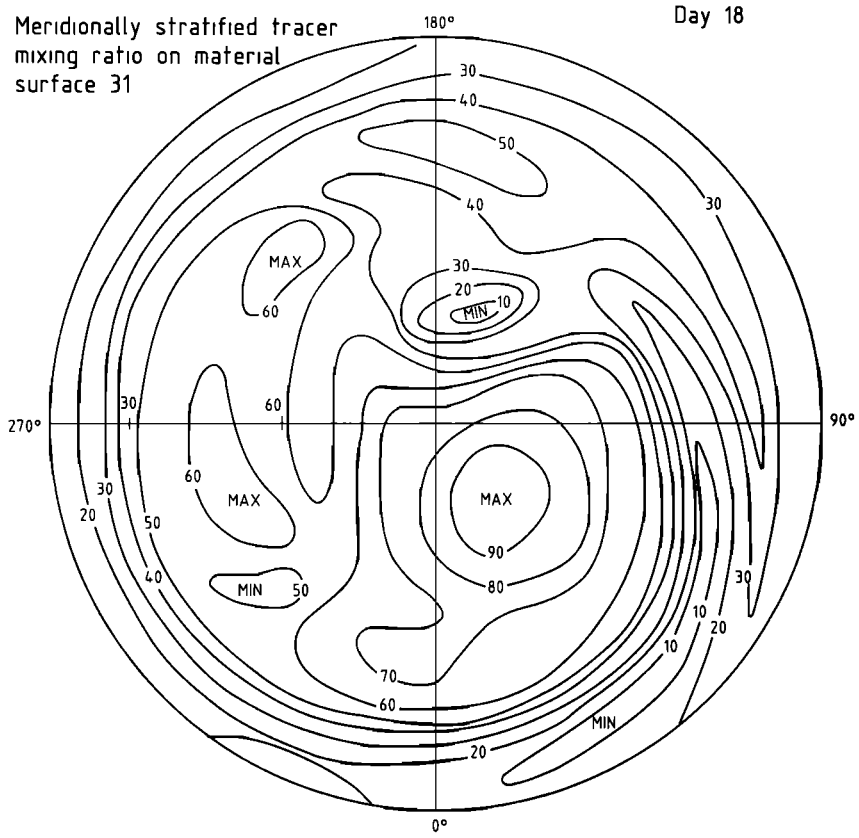
Meridionally stratified tracer
mixing ratio on material
surface 31
Day 18
180°
270°
90°
0°
MAX
MIN
30
40
50
60
20
10
70
80
90

Fig. 9*e*.

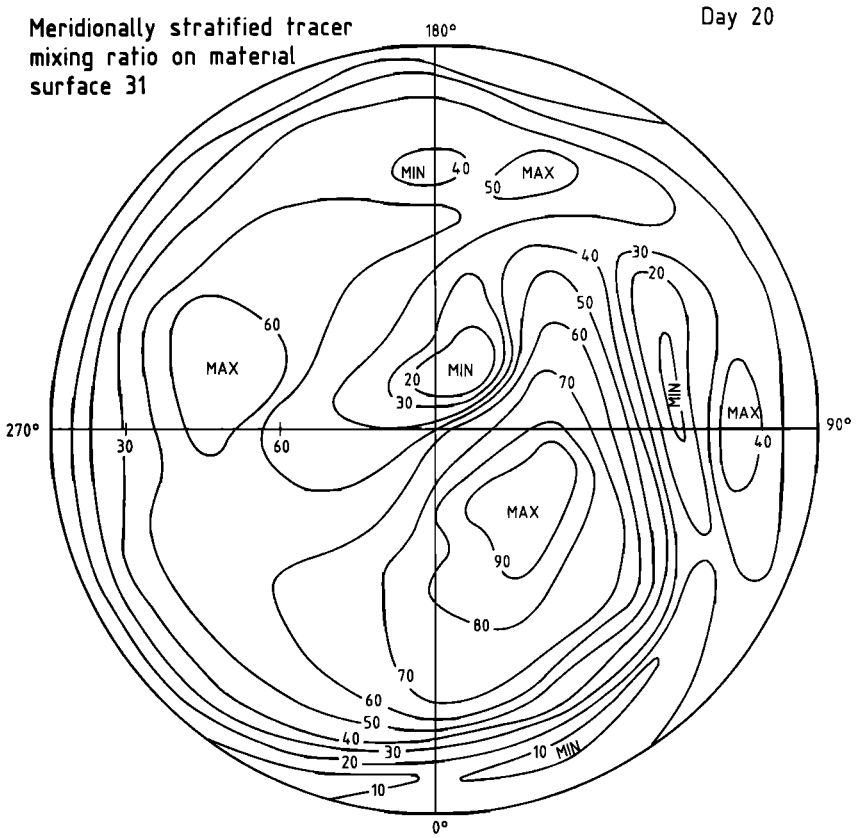
Meridionally stratified tracer
mixing ratio on material
surface 31
Day 20
180°
270°
90°
0°
MAX
MIN
30
40
50
60
20
10
70
80
90

Fig. 9*f*.

A number of quasi-conservative quantities are characterized by well-noted meridional gradients. This is the case, for example, for the ozone mixing ratio, which decreases by about a factor of 2 between the equator and the pole at 5–10 mbar. In the case of HNO_3 the mixing ratio increases by almost a factor of 4 between 0 and 90° latitude at 10–50 mbar. Finally, the Ertel's potential vorticity, which is a quasi-conservative quantity on isentropic surfaces, also increases significantly between the equator and the pole. To a first approximation the "meridionally stratified tracer" is expected to simulate, in the lower stratosphere, the behavior of such tracers. The values adopted here for the mixing ratio, namely, from 1 to 100, are obviously not representative of any physical quantity, but when irreversible mixing is weak, they should be regarded as labels to indicate the originating latitude of the air parcels. Atmospheric regions in which, for example, the mixing ratio is less than 30 are filled with air of subtropical origin.

The second gas is uniformly distributed in the horizontal at the initial stage. Its mixing ratio varies, however, linearly with height from a value of 1 at the lower boundary (10 km) to a value of 100 at the upper boundary (80 km). This tracer will be referred to as the "vertically stratified tracer," which can be associated to the potential temperature, assuming that diabatic processes are weak.

As the planetary waves develop in the model simulation in response to tropospheric forcing, the surface on which the tracers have a constant mixing ratio becomes progressively distorted. The altitude of the surface on which the mixing ratio of the "vertically stratified tracer" is 31 (originally a horizontal surface located near the 10-mbar level) is shown in Figures 9*a*, 9*b*, and 9*c* for days 15, 18, and 20 of the model integration. On day 15, for example, as the warming event develops, differences of as much as 3 km are seen in the height of this surface. The high altitudes are found at low latitudes, and the deepest sinking of the surface is located near the pole, exactly where the warming takes place as a result of adiabatic compression. The structure of this material surface is an indication of a slight upward transport at low latitude and a strong downward transport in the warm cell localized at high latitude. The same type of structure is observed in the subsequent days but with a large distortion in the initially horizontal surface. Such downward motion in the polar region is expected to generate significant vertical advective transport of constituents whose mixing ratio varies with altitude (e.g., ozone).

The meridional (or quasi-meridional) transport can be investigated by analyzing the distribution of the meridionally stratified tracer on one of the material surfaces discussed above. Any air parcel located on such a surface at the initial stage of the integration remains on this surface, since the two tracers are entirely conservative. Air with a low mixing ratio for the meridionally stratified tracer has its origin in the subtropical regions. Air with a high mixing ratio characterizes polar air. From Figures 5*a*, 5*b*, and 5*c*, which show the distribution of the geopotential on the 11.6-mbar pressure surface, and 9*d*, 9*e*, and 9*f*, which represent the mixing ratio of the meridionally stratified tracer on a material surface on which the mixing ratio of the vertically stratified tracer is 31, one clearly sees that the isohypses and the lines of constant mixing ratio (meridionally stratified tracer) are nearly parallel. The air of polar origin is thus displaced together with the polar vortex, which thus behaves as a material entity. Since the mixing ratio in the center of the displaced vortex exceeds values of 90 until the final stage of the warming, this displacement is largely reversible, and essentially no mixing takes place in the center of the vortex. This behavior was also recently noted by *Rose* [1986]. At the south edge of the vortex, opposite to the "Aleutian high," a steep gradient in the mixing ratio of the meridionally stratified tracer is visible. A similar sharp latitudinal variation has been observed at certain occasions in the amount of nitrogen dioxide [*Noxon*, 1979; *Mount et al.*, 1984]. This "Noxon cliff" has been interpreted by *Solomon and Garcia* [1983] as being related to the presence of large planetary waves and to chemical conversion processes involving N_2O_5. It has also been simulated in the three-dimensional model of *Brasseur and Rose* [1985], which includes a detailed scheme of chemical and photochemical reactions. The presence of sharp latitudinal gradients can, however, be generated even in a pure dynamical model simulation where chemical relaxation is ignored.

As the polar vortex is removed from the north pole, tongues of subtropical air move counterclockwise around the displaced vortex and transport the air parcels toward high-latitude regions. Such narrow tongues of subtropical air are observed in the ozone and nitric acid maps provided by the LIMS instrument on board the Nimbus 7 satellite [*Leovy et al.*, 1985; J. M. Russell III, private communication, 1984].

The model also predicts tongues of air moving clockwise around the vortex and transporting polar air towards mid-latitude regions. These structures are localized in a region where the geopotential is relatively uniform. When comparing the situations from day 15 to 20, it appears that these tongues of polar air become progressively irregular and even break into smaller-scale structures. This behavior was found in charts of the Ertel's potential vorticity for real atmosphere data [*McIntyre and Palmer*, 1983, 1984] and suggests some irreversible mixing associated with nonlinear processes, especially in the western hemisphere, where a wide area with weak gradients can be observed (see, in particular, Figures 9*e* and 9*f*). The model thus simulates the existence of a large "surf zone," introduced recently by *McIntyre and Palmer* [1983, 1984], in which planetary waves break and induce significant transport of tracers. The mixing ratio of the meridionally stratified tracer at the pole, which was originally equal to 100, is on day 20 reduced to about 50 on the material surface "31" near the 10-mbar level. On the same day, air which was initially located, for example, near 60° latitude has been transported as far south as 30° latitude in certain parts of the winter hemisphere. Subtropical air is thus obviously transported into the polar cap, while at the same time and on the same material surface (which remains quasi-horizontal), air originating from high latitudes reaches considerably lower latitudes. The first of these flows is well organized, while the second appears to break into smaller-scale parcels as a result of irreversible mixing. Further studies will investigate quantitatively the degree of irreversibility of these transport processes and will describe the behavior of the tracers when the waves die down.

The meridional distribution of the zonal mean mixing ratio of the meridionally stratified tracer on day 20 is represented in Figure 10. At low latitude, where the effect of planetary waves is weak, the transport is dominated by the flow generated by the equatorial Hadley cell, as indicated by an arrow. The tropical air is displaced upward and northward, as would be shown by a zonally averaged (two-dimensional) model simulation. At latitudes higher than 45° the zonally averaged struc-

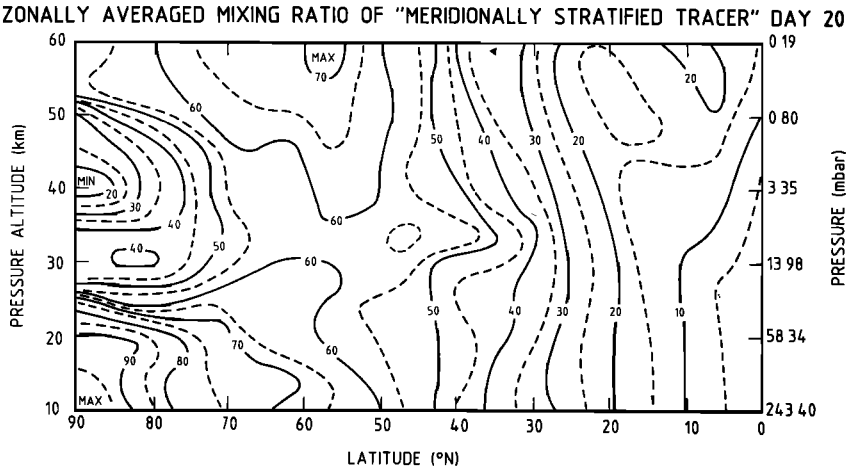

Fig. 10. Meridional cross section of the zonally averaged mixing ratio of the "meridionally stratified tracer" on day 20. The initial isolines are vertical lines.

ture of the mixing ratio appears to become very different. Values as low as 20 are found near the pole at 40 km altitude, indicating a strong convergence of subtropical air in this region. The trajectory of these air parcels cannot be inferred from this two-dimensional representation, as air with higher mixing ratio is present at mid-latitude over the entire vertical range. The zonally averaged mixing ratio of the meridionally stratified tracer at 62.5°N and 77.5°N is shown as a function of height and time in Figures 11*a* and 11*b* at all altitudes. The situation at 77.5°N does not change significantly during the early stage of the warming development (0–10 days). After day 15, as the wave activity increases, the transport of subtropical air (with low mixing ratio) becomes strong, and the zonally averaged mixing ratio of the meridionally stratified tracer decreases to less than 30. A similar situation is observed at 62.5°N. At this latitude, however, the zonally averaged mixing ratio is never smaller than 50. This might seem paradoxal, since the subtropical air (mixing ratio less than 40) which accumulates in the polar region has to flow through the mid-latitude zones before reaching the polar cap. In fact, as shown by the synoptic charts (Figures 9*d*, 9*e*, and 9*f*), the transport of subtropical air which takes place during the warming event is confined in a narrow band which behaves as a spiral around and up to the pole. This very localized flow is sufficient to fill the polar cap with subtropical air within a few days because of the spherical geometry of the earth. Such a narrow tongue does not significantly influence the value of the zonally averaged mixing ratio of the meridionally stratified tracer at mid-latitude. This type of behavior as well as the planetary wave breaking in the "surf zone" appear to be the most important processes which describe the transport in winter when the eddy perturbations are large. Such phenomena cannot be reproduced in two-dimensional model calculations but require full three-dimensional simulations.

The above study of the behavior of meridionally and vertically stratified tracers suggests that the transport of atmospheric long-lived species (O_3, HNO_3, CH_4, N_2O, chlorofluorocarbons) can be understood in terms of vertical advection, especially in the polar regions and horizontal eddy processes. The transport of species such as ozone into the polar latitudes during winter is mainly accomplished by the action of large-scale horizontal eddies. Such behavior is confirmed by *Wu et al.* [1985], who have calculated the several contributions to the ozone transport from the Nimbus 7 solar backscatter ultraviolet (SBUV) data. This study also shows that more ozone is transported into the polar region on disturbed days than on quiet days. As major warmings occur only in the northern hemisphere, the above discussion does not apply to the southern high-latitude regions. In the southern hemisphere, indeed, the polar vortex remains a very stable material entity, so that ozone can hardly penetrate into the regions closest to the pole. This should be taken into consideration when explaining the very low ozone amount observed in the Antarctica by *Farman et al.* [1985].

6. Summary and Conclusions

We have developed a three-dimensional dynamical model for the winter hemisphere which simulates the response of the middle atmosphere to a wave number 1 forcing applied near the tropopause. As the planetary waves grow and propagate in the stratosphere, the zonal mean flow decelerates, generating a strong meridional circulation and a significant heating at high latitudes. After about 18 days of model simulation the mean zonal wind at high latitude is reversed from westerly to easterly, inducing a major stratospheric warming event.

During these large-scale disturbances, subtropical air parcels in the middle stratosphere are transported toward the pole along quasi-horizontal material surfaces, and at the same time, polar air reaches regions at mid and low latitudes. This transport is far from being uniform in space. The poleward flow, for example, is confined essentially into a narrow tongue that twists as a spiral around the winter vortex, which is displaced from the pole during the warming event. Such behavior appearing in the model simulation is also visible in the ozone distribution inferred from satellite observations [*Leovy et al.*, 1985]. Moreover, in the "surf zone," nonlinear processes produce a cascade of smaller-scale structures, leading to irreversible mixing. The strength of the meridional transport is also expected to be highly variable in time. It will be enhanced at certain periods, during which the polar vortex is disturbed and eventually breaks down. Such behavior is clearly seen on the charts of ozone and nitric acid derived, for example, from the LIMS experiment. It cannot, however, be properly reproduced in zonally averaged models, even if the transport in these models is described in terms of transformed eulerian mean meridional circulation. Zonally averaged calculations are very

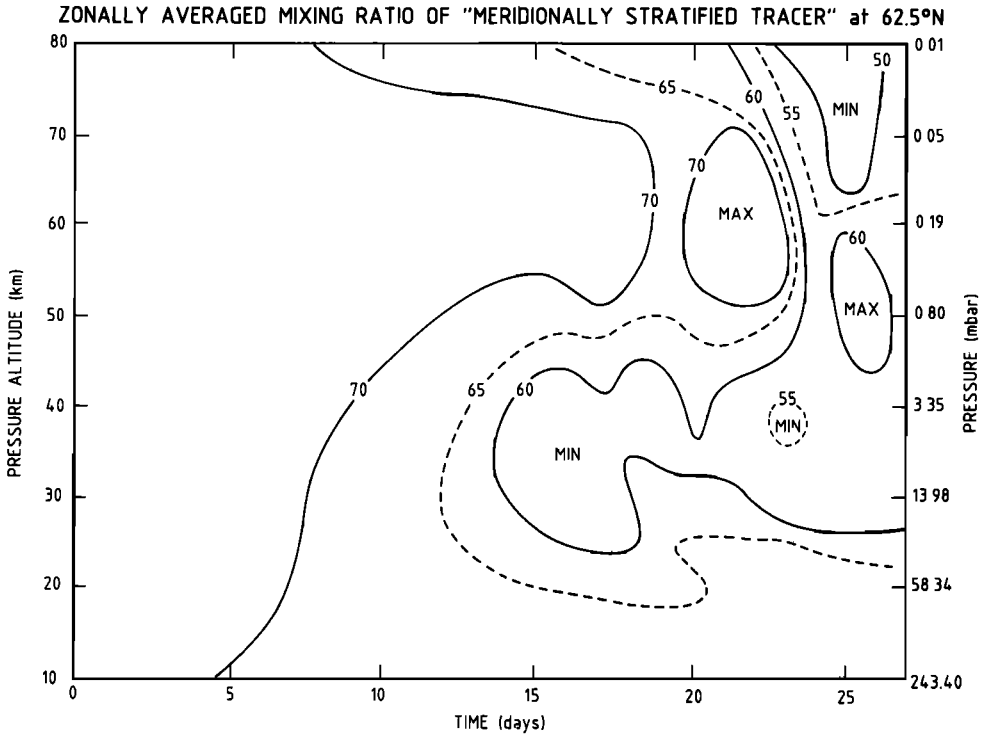

Fig. 11*a*.

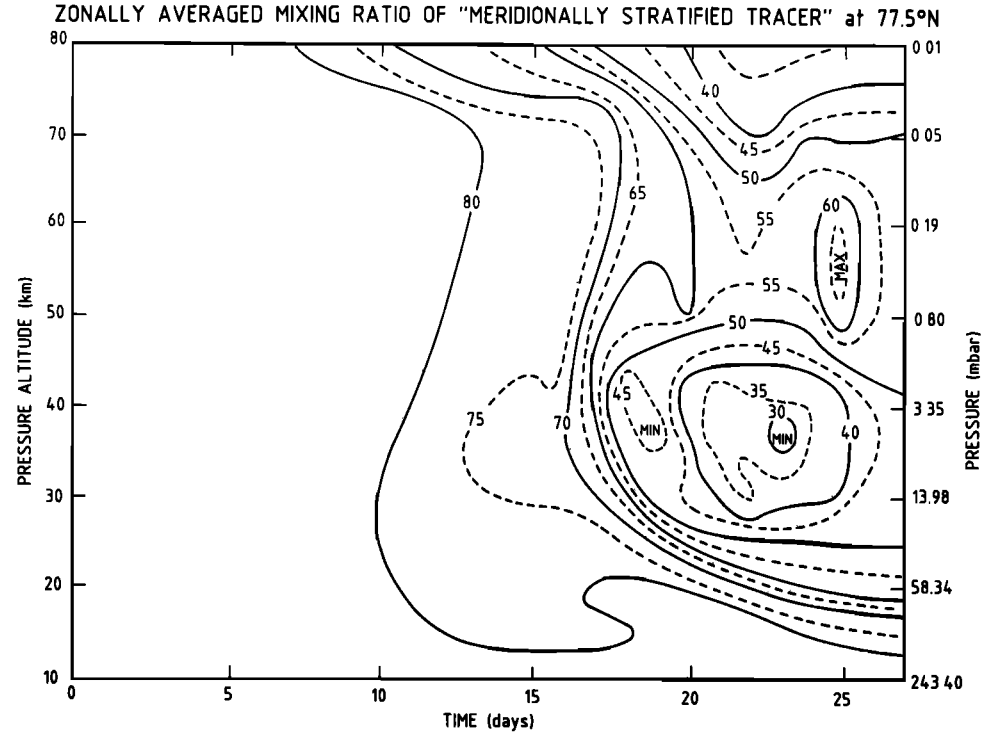

Fig. 11*b*.

Fig. 11. Time-height cross section of the zonally averaged mixing ratio of the "meridionally stratified tracer" (*a*) at 62.5°N and (*b*) 77.5°N latitude.

useful to simulate the long-term behavior of chemical species, especially when the atmosphere is not or is only slightly disturbed by planetary waves. They are no longer appropriate, either to study the detailed physical processes leading to poleward motions or to simulate the meridional transport of trace species, when large disturbances occur. Indeed, the transport becomes particularly strong when nonlinear, nonconservative, and nonsteady wave disturbances occur; that is when the approximations associated with the two-dimensional model formulation tend to fail.

Acknowledgments. The authors are indebted to the scientists of the Stratospheric Research Group at the Free University of Berlin for helpful discussions. The work was performed when the authors were visiting the Max Planck Institute for Chemistry in Mainz, Federal Republic Germany, while on leave from the Space Aeronomy Institute in Brussels, Belgium. Special thanks are due to P. Crutzen for this efficient support and his interest in this study. This work was partly supported by the Chemical Manufacturers Association under contract 84-505, and by the National Aeronautics and Space Administration under contract W-16215. The National Center for Atmospheric Research is sponsored by the National Science Foundation.

REFERENCES

Andrews, D. G., and M. E. McIntyre, Planetary waves in horizontal and vertical shear: The generalized Eliassen-Palm relation and the mean zonal acceleration, *J. Atmos. Sci.*, *33*, 2031–2048, 1976.

Andrews, D. G. and M. E. McIntyre, An exact theory of nonlinear waves in a Lagrangian–mean flow, *J. Fluid Mech.*, *89*, 609–646, 1978.

Brasseur, G., and M. Bertin, Distribution and circulation of stratospheric ozone in the meridional plane as given by a two-dimensional model, in *Proceedings of the Quadriennal Ozone Symposium, Dresden, German Democratic Republic*, pp. 297–308, Nationalkomitee für Geodäsie und Geophysik bei der Akademie der Wissenschaften der Deutschen Demokratischen Republik, 1977.

Brasseur, G., and M. Bertin, The action of chlorine on the ozone layer as given by a zonally averaged two-dimensional model, *Pure Appl. Geophys.*, *117*, 437–447, 1979.

Brasseur, G., and K. Rose, Ozone and nitrogen oxides in the middle atmosphere: A three-dimensional model simulation, Proceedings of the 7th ESA Symposium on European Rocket and Balloon Programmes and Related Research, *Eur. Space Agency Spec. Publ., ESA SP-229*, 1985.

Brewer, A. W., Evidence for a world circulation provided by measurements of helium and water vapour distribution in the stratosphere, *Q. J. R. Meteorol. Soc.*, *75*, 351–363, 1949.

Charney, J. G., and P. G. Drazin, Propagation of planetary-scale disturbances from the lower into the upper atmosphere, *J. Geophys. Res.*, *66*, 83–109, 1961.

Crutzen, P. J., A two-dimensional photochemical model of the atmosphere below 55 km: Estimates of natural and man-caused ozone perturbations due to NO_x, Proceedings of 4th Conference on the Climatic Impact Assessment Program, *DOT-TSC-OST-38*, U.S. Dep. of Transp., Washington D. C., 1975.

Cunnold, D., F. Alyea, N. Phillips, and R. Prinn, A three-dimensional dynamical chemical model of atmospheric ozone, *J. Atmos. Sci.*, *32*, 170–194, 1975.

Cunnold, D. M., F. N. Alyea, and R. G. Prinn, Preliminary calculations concerning the maintainance of the zonal mean ozone distribution in the northern hemisphere, *Pure Appl. Geophys.*, *118*, 329–354, 1980.

Dobson, G. M. B., Origin and distribution of polyabonic molecules in the atmosphere, *Proc. R. Soc. London, Ser. A*, *236*, 187–193, 1956.

Dunkerton, T. J., On the mean meridional mass motions of the stratosphere and mesosphere, *J. Atmos. Sci.*, *35*, 2325–2333, 1978.

Dunkerton, R., C.-P. F. Hsu, and M. E. McIntyre, Some eulerian and lagrangian diagnostics for a model stratospheric warming, *J. Atmos. Sci.*, *38*, 819–843, 1981.

Farman, J. C., B. G. Gardiner, and J. D. Shanklin, Large losses of total ozone in Antarctica reveal seasonal ClO_x/NO_x interaction, *Nature*, *315*, 207–210, 1985.

Garcia, R. R., and D. L. Hartmann, The role of planetary waves in the maintenance of the zonally averaged ozone distribution in the upper stratosphere, *J. Atmos. Sci.*, *37*, 2248–2264, 1980.

Garcia, R. R., and S. Solomon, A numerical model of the zonally averaged dynamical and chemical structure of the middle atmosphere, *J. Geophys. Res.*, *88*, 1379–1400, 1983.

Ghazi, A., Nimbus 4 observations in total ozone and stratospheric temperature during a sudden warming, *J. Atmos. Sci.*, *31*, 2197–2206, 1974.

Ghazi, A., A. Ebel, and D. F. Heath, A study of satellite observations of ozone and stratospheric temperature during 1970–1971, *J. Geophys. Res.*, *81*, 5365–5373, 1976.

Gille, J. C., Middle atmosphere processes revealed by satellite observations, *J. Atmos. Terr. Phys.*, *41*, 707–722, 1979.

Guthrie, P. D., C. H. Jackman, J. R. Herman, and C. J. McQuillan, A diabatic circulation experiment in a two-dimensional photochemical model, *J. Geophys. Res.*, *89*, 9589–9602, 1984.

Hartmann, D. L., and R. R. Garcia, A mechanistic model of ozone transport by planetary waves in the atmosphere, *J. Atmos. Sci.*, *36*, 350–364, 1979.

Harwood, R. S., and J. A. Pyle, A two-dimensional mean circulation model for the atmosphere below 80 km, *Q. J. R. Meteorol. Soc.*, *101*, 723–747, 1975.

Hesstvedt, E., The effects of supersonic transport upon the ozone layer studied in a two-dimensional photochemical model with transport, Item 6, *AGARD Conf. Proc. AGARD-CP-125*, 1973.

Holton, J. R., *The Dynamic Meteorology of the Stratosphere and Mesosphere*, *Meteorol. Mongr.*, *37*, 218 pp., American Meteorological Society, Boston, Mass., 1975.

Holton, J. R., A semi-spectral numerical model for wave, mean-flow interactions in the stratosphere: Application to sudden stratospheric warmings, *J. Atmos. Sci.*, *33*, 1639–1649, 1976.

Holton, J. R., The dynamics of sudden stratospheric warmings, *Annu. Rev. Earth Planet. Sci.*, *8*, 169–190, 1980.

Holton, J. R., An advective model for two-dimensional transport of stratospheric trace species, *J. Geophys. Res.*, *86*, 11,989–11,994, 1981.

Hsu, C.-P. F., Air parcel motions during a numerically simulated sudden stratospheric warming, *J. Atmos. Sci.*, *37*, 2768–2792, 1980.

Hunt, B. G., and S. Manabe, Experiments with a stratospheric general circulation model: II, The large-scale diffusion of tracers in the stratosphere, *Mon. Weather Rev.*, *96*, 305–339, 1968.

Kawahira, K., A quasi-one-dimensional model of the ozone transport by planetary waves in the winter stratosphere, *J. Meteorol. Soc. Jpn.*, *60*, 831–849, 1982.

Kida, H., A numerical investigation of the atmospheric general circulation and stratospheric-tropospheric mass exchange: I, Long-term integration of simplified general circulation model; II, Lagrangian motion of the atmosphere, *J. Meteorol. Soc. Jpn.*, *55*, 52–88, 1977.

Kida, H. General circulation of air parcels and transport characteristics derived from a hemispheric GCM, 1, A determination of advective mass flow in the lower stratosphere, *J. Meteorol. Soc. Jpn.*, *61*, 510–523, 1983.

Ko, M. K. W., K. K. Tung, D. K. Weinstein, and N. D. Sze, A zonal-mean model of stratospheric tracer transport in isentropic coordinates: Numerical simulations for nitrous oxide and nitric acid, *J. Geophys. Res.*, *90*, 2313–2329, 1985.

Leovy, C. B., C.-R. Sun, M. H. Hitchman, E. E. Remsberg, J. M. Russell III, L. L. Gordley, J. C. Gille, and L. V. Lyjak, Transport of ozone in the middle stratosphere: Evidence for planetary wave breaking, *J. Atmos. Sci.*, *42*, 230–244, 1985.

Levy, H. II, J. D. Mahlman, and W. J. Moxim, A preliminary report on the numerical simulation of the three-dimensional structure and variability of atmospheric N_2O, *Geophys. Res. Lett.*, *6*, 155–158, 1979.

Louis, J. F., A two-dimensional transport model of the atmosphere, Ph.D. thesis, Univ. of Color., Boulder, 1974.

Mahlman, J. D., and W. J. Moxim, Tracer simulation using global general circulation model: Results from a mid-latitude instantaneous source experiment, *J. Atmos. Sci.*, *35*, 1340–1374, 1978.

Mahlman, J. D., H. Levy II, and W. J. Moxim, Three-dimensional tracer structure and behavior as simulated in two ozone precursor experiments, *J. Atmos. Sci.*, *37*, 655–685, 1980.

McIntyre, M. E., and T. N. Palmer, Breaking planetary waves in the stratosphere, *Nature*, *305*, 593–600, 1983.

McIntyre, M. P., and T. N. Palmer, The "surf zone" in the stratosphere, *J. Atmos. Terr. Phys.*, *46*, 825–850, 1984.

Miller, C., D. L. Filkin, A. J. Owens, J. M. Steed, and J. P. Jesson, A two-dimensional model of stratospheric chemistry and transport, *J. Geophys. Res.*, *86*, 12,039–12,065, 1981.

Mount, G. H., D. W. Rusch, J. F. Noxon, J. M. Zawodny, and C. A. Barth, Measurements of stratospheric NO_2 from the Solar Mesosphere Explorer, 1, An overview of the results, *J. Geophys. Res.*, *89*, 1327–1340, 1984.

Murgatroyd, R. J., and F. Singleton, Possible meridional circulation in the stratosphere and mesosphere, *Q. J. R. Meteorol. Soc.*, *87*, 125–135, 1961.

Noxon, J. F., Stratospheric NO_2, 2, Global behavior, *J. Geophys. Res.*, *84*, 5067–5076, 1979.

Petzoldt, K., and M. Scholl, The role of the potential vorticity gradi-

ent for the breakdown of the zonal flow in the stratosphere and mesosphere during February 1980, *Contrib. Atmos. Phys.*, *59*, 301–320, 1986.

Pyle, J. A., and C. F. Rogers, A modified diabatic circulation model for stratospheric tracer transport, *Nature*, *287*, 711–714, 1980.

Reed, R. J., and K. E. German, A contribution to the problem of stratospheric diffusion by large-scale mixing, *Mon. Weather Rev.*, *93*, 313–321, 1965.

Rose, K., On the influence of nonlinear wave-wave interaction in a 3-D primitive equation model for sudden stratospheric warmings, *Contrib. Atmos. Phys.*, *56*, 14–41, 1983.

Rose, K., The stratospheric winter polar vortex simulated as a material entity, *J. Atmos. Terr. Phys.*, in press, 1986.

Rose, K., and G. Brasseur, Ozone during a sudden stratospheric warming: A three-dimensional simulation, in *Atmospheric Ozone, Proceedings of the Quadrennial Ozone Symposium, Halkidiki, Greece*, edited by C. S. Zerefos and A. Ghazi, D. Reidel, Hingham, Mass., 1985.

Schlesinger, M. E., and Y. Mintz, Numerical simulation of ozone production, transport and distribution with a global atmospheric general circulation model, *J. Atmos. Sci.*, *36*, 1325–1361, 1979.

Shapiro, R., The use of linear filtering as a parameterization of atmospheric diffusion, *J. Atmos. Sci.*, *28*, 523–531, 1971.

Solomon, S., and R. R. Garcia, Simulation of NO_x partitioning along isobaric parcel trajectories, *J. Geophys. Res.*, *88*, 5497–5501, 1983.

Stordal, F., I. S. A. Isaksen, and K. Horntveth, A diabatic circulation two-dimensional model with photochemistry: Simulations of ozone and long-lived tracers with surface sources, *J. Geophys. Res.*, *90*, 5757–5776, 1985.

Tung, K. K., On the two-dimensional transport of stratospheric trace gases in isentropic coordinates, *J. Atmos. Sci.*, *39*, 2330–2355, 1982.

Vincent, D. G., Mean meridional circulations in the northern hemisphere lower stratosphere during 1964 and 1965, *Q. J. R. Meteorol. Soc.*, *94*, 333–349, 1968.

Whitten, R. C., W. J. Borucki, V. R. Watson, T. Shimazaki, H. T. Woodward, C. A. Riegel, L. A. Capone, and T. Becker, The NASA Ames Research Center one- and two-dimensional stratospheric models, 2, Two-dimensional model, *NASA Tech. Pap. 1003*, 1977.

Wu, M. F., M. A. Geller, J. G. Olson, A. J. Miller, and R. M. Nagatani, Computations of ozone transport using Nimbus 7 solar backscatter ultraviolet and NOAA/National Meteorological Center data, *J. Geophys. Res.*, *90*, 5745–5755, 1985.

G. Brasseur, National Center for Atmospheric Research, P.O. Box 3000, Boulder, CO 80307.

W. Kouker, Max Planck Institute for Chemistry, P. O. Box 3060, 6500 Mainz, Federal Republic of Germany.

(Received February 27, 1986;
revised June 24, 1986;
accepted June 30, 1986.)